International Journal of Control, Automation and Systems, Vol. 15, Issue 4, August 2017, pp. 1969-1974
DOI:10.1007/s12555-016-0109-4

Title of the paper

Efficient Aimpoint Tracking Using Target Range Profiles of a Wideband FMCW Seeker

Title of the publication

(to which this paper is submitted)

International Journal of Control, Automation, and Systems

Authors

Won-Sang Ra, School of Mechanical and Control Engineering, Handong Global Univ.,
558 Handong-ro, Pohang, Gyeongbuk, 37554, Korea,
E-mail : wonsang@handong.edu

Ick-Ho Whang, Guidance and Control Department, Agency for Defense Development,
P.O. Box 35, Daejeon 34186, Korea,
E-mail : ickho@add.re.kr

Hyo-Sang Shin, Centre for Autonomous and Cyberphysical Systems, Cranfield Univ.,
College Road, Cranfield, MK43 0AL, U.K.,
E-mail : h.shin@cranfield.ac.uk

Antonios Tsourdos, Centre for Autonomous and Cyberphysical Systems, Cranfield Univ.,
College Road, Cranfield, MK43 0AL, U.K.,
E-mail : a.tsourdos@cranfield.ac.uk

Abstract

This paper proposes an efficient aimpoint tracking filter for high-range resolution FMCW radar seekers. A modified probabilistic data association scheme is devised to deal with closely located measurements generated by scatterers of an extended target and multipath clutter. In order to discriminate the aimpoint measurements from others, an approximate target range profile is used for calculating likelihoods of the validated measurements. Simulation results show the effectiveness and performance of the proposed approach.

1 Introduction

The surface-to-air missile(SAM) system has been developed as a layered defense to defeat all ranges of threats from aerial targets [1–3]. As an efficient way for intercepting highly maneuvering aerial targets, a hit-to-kill requirement has the increasing importance in modern SAMs [1]. To make the hit-to-kill guidance feasible, it is desirable to adopt a high-range resolution(or wideband) radar seeker which provides not only the kinematic states of an aerial target but also its size and shape. The additional target information is very useful to analyze the vulnerability of an aerial target and precisely track an aimpoint of target interception as well [4–6]. Nevertheless, very few research results on this issue have been available so far.

The target tracking using a wideband FMCW radar seeker is inherently accompanied by a difficult data association problem. Unlike a narrowband radar seeker which recognizes a target as a single object, a wideband seeker potentially offers multiple measurements corresponding to individual scatterers within the target extent [7]. It leads to the complex radar cross section(RCS) characteristics of a target due to multiple closely located scatterers, which make the target tracking problem complicated. To have a good grasp on this problem, it is necessary to understand the typical signal processing scheme of the FMCW radar seekers based on the triangular frequency modulation technique [8, 9]. The seeker receives signals originated from scatterers at interested sections of an aerial target and calculates its power spectrum in each up and down chirp period [10]. The frequency with maximum power is usually defined as the target frequency measurement under the assumption that the power of an interested scatterer is dominant compared to others. Then, its relative range and range rate are obtained by associating the frequency measurements in each chirp period [8]. However, this conventional measurement generation principle could not be applied for extended target tracking using wideband seekers. This is because, if there exist multiple target measurements, numerous local peaks of the power spectrum appear in each chirp period. For such case, a well-defined association logic is required for target detection.

Meanwhile, the complex RCS characteristics of an aerial target is an another factor making the problem more difficult. As shown in Fig. 1, the RCS of an

aerial target tends to be mainly determined by its nose, body and tail sections. The main scatterers are close to each other, thus they have very similar values of range and range rate with respect to the seeker. Besides, if the aimpoint of an aerial target has the smaller RCS value than the others or even the target detection threshold, it might not be detected in occasion. Therefore, the aimpoint tracking using wideband FMCW seeker can be cast into the target tracking problem with multiple adjacent measurements and a relatively small detection probability as well. Unfortunately, closely located multiple measurements might severely deteriorate the aimpoint tracking performance of the conventional data association filters.

To tackle the above mentioned problems, a precise aimpoint tracking filter is developed in range-Doppler domain. The main idea of the proposed approach is to consider an approximated target range profile and to modify the association probability of the conventional probabilistic data association(PDA) scheme in [11]. If the typical length of an arieal target are roughly known from a wideband seeker, the *a priori* information on kinematic relation between dominant radar scatterers can be generated and the most probable position of an aimpoint can be guessed as well [12]. Since the aimpoint measurements are randomly distributed around the predicted aimpoint, the aimpoint appearance is described as a likelihood function. To effectively separate the aimpoint measurement from others, the data association procedure of the existing PDA filter(PDAF) is redefined using our approximate target range profile. In consequence, the proposed filter shows the reliable aimpoint tracking performance even when the aimpoint detection probability is relatively low. Moreover, the proposed aimpoint tracking algorithm can be implemented in real-time because of its simple filter structure.

2 System Model for Filter Design in Range-Doppler Domain

2.1 Measurement Model

Once the time delay between transmitted and received signals of a FMCW radar based on triangular modulation is converted to a frequency differences(or beat frequencies) as shown in Fig. 2, the target range and range rate measurements are obtained from the beat frequencies.

The transmitted signal is assumed as

$$s_T(t) = A_T \cos(\varphi_T(t)), \tag{1}$$

where t is the continuous time index. A_T and φ_T are the gain and phase of the transmitted sinusoidal signal, respectively. The frequency of the transmitted signal in the FMCW radar is linearly varied in each chirp period. For $t \in [-T_s/2, T_s/2)$,

$$f_T(t) = f_c + s_c \frac{B}{T_s} t, \quad s_c \triangleq \begin{cases} +1, & \text{up-chirp} \\ -1, & \text{down-chirp} \end{cases}. \tag{2}$$

In the above, f_c is the center frequency, B is the sweep bandwidth and T_s is the sweep time.

Integrating (2) from $-T_s/2$ to t yields the phase of $s_T(t)$.

$$\varphi_T(t) \triangleq 2\pi \int_{-\frac{T_s}{2}}^{t} f_T(t)dt = 2\pi \left(f_c\, t + s_c \frac{1}{2} \frac{B}{T_s} t^2 \right) - \varphi_0, \tag{3}$$

where φ_0 denotes an integration constant.

For the FMCW radar seeker with conventional superheterodyne receiver, the received signal goes through the mixer and then is amplified in the intermediate frequency(IF) band. The received signal is used as the reference signal to detect target reflection signal and frequency. By passing the received signal within the IF band through the mixer again, the beat signal s_b is obtained.

$$s_b(t) = A_b \cos(\Delta\varphi_b(t)), \quad \Delta\varphi_b(t) = \varphi_T(t) - \varphi_T(t-\tau) \tag{4}$$

In the above equation, A_b and $\Delta\varphi_b$ are the gain and phase of the beat signal, respectively. $\tau = 2\frac{R+\dot{R}t}{c}$ is the time delay between the transmitted and received signal where R and $\dot{R}$ mean the range and range rate. c is the speed of light.

If $\frac{\tau}{T_s} \ll 1$ and the range-range rate coupling is negligible, the phase of the beat signal is approximated as

$$\Delta\varphi_b(t) \approx 2\pi \left[\frac{2f_c R}{c} + \left(s_c \frac{2BR}{T_s c} + \frac{2f_c \dot{R}}{c} \right) t \right] \tag{5}$$

Thus, the beat frequency is obtained according to

$$f_b \triangleq \frac{d}{dt}\Delta\varphi_b(t) \approx s_c \frac{2BR}{T_s c} + \frac{2f_c \dot{R}}{c} \tag{6}$$

Finally, the measurement equation is derived as follows:

$$y_k \;=\; H_k \boldsymbol{x}_k + v_k. \tag{7}$$

Letting the target acceleration in vertical plane be a_z^t, the target state vector $\boldsymbol{x}$, the measurement y, and the measurement matrix H in the above equation are

$$\boldsymbol{x} \triangleq \begin{bmatrix} R & \dot{R} & a_z^t \end{bmatrix}^T, \quad y \triangleq f_b, \quad H \triangleq \begin{bmatrix} s_c \frac{2B}{T_s c} & \frac{2f_c}{c} & 0 \end{bmatrix}.$$

In (7), the measurement noise v is assumed as a zero-mean and is normally distributed with covariance R_v.

Note that since the distance between the dominant scatterers of an aerial target is negligible compared to the range from the SAM, the measurement model of the scatterers is regarded as approximately the same.

2.2 Target Motion Model

Let us consider the engagement geometry in the vertical plane. In Fig. 3, (X_I, Z_I) represents the inertial frame, R is the range and λ_θ is the LOS angle. $\omega_y = \dot{\lambda}_\theta$ indicates the vertical LOS rate. a_z^m, v_m, γ_m are the pitch acceleration, velocity and flight path angle of the missile. Similarly, a_z^t, v_m and γ_t are the quantities for the target. The kinematic relations are given as follows:

$$\dot{R} \;=\; v_t \cos(\gamma_t - \lambda_\theta) - v_m \cos(\gamma_m - \lambda_\theta) \tag{8}$$

$$R\omega_y \;=\; v_t \sin(\gamma_t - \lambda_\theta) - v_m \sin(\gamma_m - \lambda_\theta) \tag{9}$$

Under the piecewise constant velocity assumption, differentiating (8) and substituting (9) into the result yield

$$\begin{aligned} \ddot{R} - R\omega_y^2 \approx & v_m \sin(\gamma_m - \lambda_\theta)\dot{\gamma}_m - v_t \sin(\gamma_t - \lambda_\theta)\dot{\gamma}_t \\ = & a_z^t - a_z^m. \end{aligned} \tag{10}$$

The unknown target acceleration is modeled as

$$\dot{a}_z^t = -1/\tau_R \ \cdot a_z^t + w_R, \tag{11}$$

where τ_R is the time constant for target maneuver. w_R is the target jerk assumed to be a zero-mean white noise with variance q_R.

Using (8)$\sim$(11), the target dynamics model is written as

$$\dot{\boldsymbol{x}}(t) = A\boldsymbol{x}(t) + \boldsymbol{u}(t) + Bu^c(t) \tag{12}$$

where the unknown incremental acceleration $\boldsymbol{u}$, the known input u^c, and the relevant matrices are defined as

$$\boldsymbol{u} \triangleq \begin{bmatrix} 0 \\ 0 \\ w_R \end{bmatrix}, \ u^c = -a_z^m, \ A \triangleq \begin{bmatrix} 0 & 1 & 0 \\ \omega_y^2 & 0 & 1 \\ 0 & 0 & -\frac{1}{\tau_R} \end{bmatrix}, \ B \triangleq \begin{bmatrix} 0 \\ 1 \\ 0 \end{bmatrix}.$$

If $T/\tau_R \ll 1$, $\omega_y T \ll 1$ and $\omega_y \tau_R \ll 1$ for the signal processing time duration T of an FMCW radar seeker, the target motion model in discrete-time is obtained from (12).

$$\boldsymbol{x}_{k+1} = F\boldsymbol{x}_k + \boldsymbol{u}_k + \boldsymbol{G}^c u_k^c, \quad \boldsymbol{u}_k \sim \mathcal{N}(0, Q_k), \tag{13}$$

$$F = \begin{bmatrix} 1 & T & \frac{T^2}{2} \\ 0 & 1 & T \\ 0 & 0 & 1 \end{bmatrix}, \ \boldsymbol{G}^c = \begin{bmatrix} \frac{T^2}{2} \\ T \\ 0 \end{bmatrix}, \ Q = q_R \begin{bmatrix} \frac{T^5}{20} & \frac{T^4}{8} & \frac{T^3}{6} \\ \frac{T^4}{8} & \frac{T^3}{3} & \frac{T^2}{2} \\ \frac{T^3}{6} & \frac{T^2}{2} & T \end{bmatrix}.$$

In (13), k is the discrete time index. $\mathcal{N}(\mu, \sigma^2)$ is the normal distribution with mean μ and standard deviation σ. Note that the proposed algorithm requires the standing assumption that the target motion is described by the Singer model (11). If this is not satisfied as in [13], the aimpoint tracking performance of the proposed filter could be degraded. For such case, the underlying design concept of our aimpoint tracking filter should be associated with the existing target maneuver detection techniques based on an interacting multiple model tracking, multiple hypotheses tracking, and so on [14].

3 Aimpoint Tracking Filter Using an Approximate Target Range Profile

This section introduces an aimpoint measurement appearance model used for enhancing the performance of the conventional PDAF and outlines the proposed

aimpoint tracking algorithm. For convenience, the aimpoint is set as the nose section of an aerial target but it is changeable.

The following assumptions are made in order to develop an approximate measurement appearance model associated with the target range profile given by a seeker.

A1. The measurement corresponding to the peak power spectrum is usually originated from the body center of an aerial target as shown in Fig. 1.

A2. The range difference d_n between aimpoint(nose) and body center is modeled as the Gaussian distribution with mean $\bar{d}_n$ and variance σ_n^2: $d_n \sim \mathcal{N}(\bar{d}_n, \sigma_n^2)$.

From Fig. 1, the measurements corresponding to the peak power spectrum are mostly originated from the body center or the tail. The assumption A1 is reasonable since, through the validation process in the PDAF, the tail measurement is discarded from other measurements. The parameters $\bar{d}_n$ and σ_n^2 required for A2 are regarded as known constants because these can be calculated using the additional target information provided by a wideband radar seeker [12]. For instance, $\bar{d}_n$ is readily calculated from the length of a target. When a target with length L is approaching, the range difference between aimpoint and body center section could be approximated as $\bar{d}_n \approx -L/2$. σ_n reflects the error of the above approximation.

Based on A1 and A2, the aimpoint measurement appearance is approximated as follows:

$$\begin{aligned} p_n(y(i)) &= |2\pi\sigma_f^2|^{-1/2} \cdot e^{-\frac{1}{2\sigma_f^2}(y(i)-\hat{y}_n)^2}, \quad i = 1 \sim N_y, \\ \hat{y}_n &= y_{peak} - s_{\dot{R}} s_c \tfrac{2B}{Tc} \bar{d}_n, \\ s_{\dot{R}} &= \begin{cases} +1, & \dot{R} > 0 \quad \text{(receding target)} \\ -1, & \dot{R} \le 0 \quad \text{(approaching target)} \end{cases} \end{aligned} \tag{14}$$

In (14), $y(i)$ is ith frequency measurement obtained from FMCW radar seeker. N_y is the number of measurements. σ_f is the standard deviation of the frequency measurement noise, which is computed as $\sigma_f = \frac{2B}{Tc}\sigma_n$. $\hat{y}_n$ is the predicted aimpoint frequency measurement.

Note that y_{peak} is the frequency measurement corresponding to the peak power spectrum provided by the signal processing unit of a FMCW radar seeker and is considered to be generated by the body center of a target from the assumption A1. $\frac{2B}{Tc}\bar{d}_n$ is the difference between frequency measurements of the aimpoint and the body center. The predicted aimpoint frequency measurement $\hat{y}_n$ depends on the relative geometry. It is bigger than y_{peak} by $\frac{2B}{Tc}\bar{d}_n$ when the target approaches the seeker. On the other hand, in the case of the receding target, it is smaller than y_{peak} by $\frac{2B}{Tc}\bar{d}_n$.

From (14), our aimpoint measurement appearance model $p_n(y(i))$ provides the probability that the obtained measurement is originated from the aimpoint. It will have a large value, if the frequency measurement $y(i)$ is nearly equivalent with the predicted aimpoint frequency measurement $\hat{y}_n$ as illustrated in Fig. 4. In accordance, the aimpoint appearance model $p_n(y(i))$ serves as a likelihood function to represent whether the given measurement is similar with the aimpoint measurement.

Since there exist multi-path clutters in real situations, the probabilistic model of clutter appearance $p_c(y)$ is also taken into account. For simplicity, it is assumed to be uniformly distributed as follows:

$$p_c(y) = 1/(y_{max} - y_{min}) \tag{15}$$

In (15), y_{max} and y_{min} are regarded as the known frequencies determined by the detection region of an FMCW radar seeker. Thus, $p_c(y)$ can be computed in advance.

Now, incorporating (14) with (15) yields the following approximate measurement appearance model.

$$l(y(i)) = p_n(y(i))/p_c(y) \tag{16}$$

The measurement appearance model $l(y(i))$ facilitates the aimpoint tracking performance improvement of the conventional PDAF. This is because the aimpoint measurement can be efficiently discriminated from others by using the modified data association probability.

The proposed algorithm is summarized as follows:

1) The innovation sequence $\nu_k(i),\ i = 0 \sim N_y$ and its covariance S_k are defined using the *a priori* state estimate and its error covariance of the

Kalman filter.

$$\begin{aligned} \hat{\boldsymbol{x}}_{k|k-1} &= F\hat{\boldsymbol{x}}_{k-1|k-1}, \\ P_{k|k-1} &= FP_{k-1|k-1}F^T + Q_k, \\ \nu_k(i) &= y_k(i) - \hat{y}_{k|k-1}, \quad \hat{y}_{k|k-1} = H_k\hat{\boldsymbol{x}}_{k|k-1}, \\ S_k &= H_kP_{k|k-1}H_k^T + R_k. \end{aligned} \tag{17}$$

2) The measurement validation is performed to eliminate measurements which are less likely to be originated from the aimpoint section. The validated measurements satisfy the constraint (18) where γ is the threshold for measurement validation.

$$\mathcal{V}(k,\gamma) = \{y : \nu_k(i)^T S_k^{-1}\nu_k(i) \le \gamma\} \tag{18}$$

3) The association probabilities are redefined by applying the aimpoint appearance model.

$$\begin{aligned} \beta_k(i) &= \begin{cases} \dfrac{c_n}{p_c(y)}\mathcal{L}_k(i) & , \ i=1 \sim N_{vy} \\ c_n|(2\pi)^2 S_k\sigma_f^2|^{\frac{1}{2}} N_{vy}\dfrac{1-P_GP_D}{V_kP_D} & , \ i=0 \end{cases} \\ \mathcal{L}_k(i) &= \exp\left\{-\left(\frac{\nu_k(i)^2}{2S_k} + \frac{(y_k(i)-\hat{y}_n)^2}{2\sigma_f^2}\right)\right\} \end{aligned} \tag{19}$$

In (19), c_n is the normalizing constant, P_G is the gating probability, P_D is the detection probability, V_k is the volume of the measurement validation region, and N_{vy} is the number of validated measurements. $i = 0$ means all measurements are false-alarmed.

4) The measurement update is performed as in the standard PDAF.

$$\begin{aligned} \hat{\boldsymbol{x}}_{k|k} &= \hat{\boldsymbol{x}}_{k|k-1} + P_{k|k-1}H_k^T S_k^{-1} \\ P_{k|k} &= \beta_k(0)P_{k|k-1} + \big(1-\beta_k(0)\big)\big(P_{k|k-1} - W_kS_kW_k^T\big) \\ &\quad + W_k\left(\Sigma_{i=1}^{N_{vy}}\beta_k(i)\nu_k(i)^2 - \bar{\nu}_k^2\right)W_k^T \\ W_k &= P_{k|k-1}H_k^T S_k^{-1}, \quad \bar{\nu}_k = \Sigma_{i=1}^{N_{vy}}\beta_k(i)\nu_k(i) \end{aligned} \tag{20}$$

It is remarkable that the modified association probability (19) utilizes the kinematic relation between dominant scatterers to enhance the data association performance. This enables us to effectively avoid the performance deterioration of the existing aimpoint tracking filter in the cluttered environment with multiple closely located measurements.

4 Simulation Result

For the typical engagement scenario shown in Fig. 5, simulations are carried out to demonstrate the aimpoint tracking performance of the proposed algorithm. The simulation parameters are given as follows:

$$P_D = 90\%,\ P_G = 99\%,$$
$$T_0 = 1.5[sec],\ T_f = 8.0[sec],\ T = T_s = 0.01[sec],$$
$$R_v = 2.5[kHz],\ q_R = 30,\ \bar{d}_n = 3[m],\ \sigma_n = 1[m]$$

Note that the range differences between scatterers are nearly constant regardless of flight time and the range rate differences are negligible. Figure 6 shows that there are at least two measurements including clutter measurements which are uniformly distributed with detection probability of 75% and average number of 2.

The range and range rate estimation errors obtained from 100 Monte-Carlo trials are depicted in Fig. 7 and Fig. 8, respectively. For performance comparison, the nearest neighborhood filter(NNF) and the standard PDAF are simulated with the proposed method. It is clear that the existing NNF and PDAF show poor aimpoint tracking performance. As mentioned with Fig. 5, this is because the scatterers of the aerial target are closely located and the measurements originated from the body center have higher detection probability than those from the tail or the

nose. For such reasons, the standard PDAF cannot classify adjacent radar measurements and thus provides unsatisfactory aimpoint tracking results. This can also be confirmed by analyzing the residual sequences $\nu_k(i)$ within the validation gate $\mathcal{V}(k,\gamma)$ in Fig. 9. The standard PDAF validates the measurements generated from the aimpoint and the body center but it consistently confuses the body center measurement with the aimpoint measurement. In contrast, the proposed method is successful in tracking the aimpoint because it can discriminate the aimpoint measurements from others using the appearance model (14).

From a wideband seeker, coarse information about the size and/or the type of an aerial target would be provided for a SAM. Nevertheless, the standard deviation $\sigma_f \propto \sigma_n$ used in our aimpoint appearance model (14) may be uncertain

in practice. In order to check whether the proposed algorithm is robust against this uncertainty, the additional simulations are performed for $\pm 50\%$ parameter variations of σ_n. The aimpoint tracking results in Fig. 10 show that there is no noticeable performance degradation even in the
presence of the uncertainty in the parameter σ_n. It implies that the suggested method is less sensitive to the imperfectness of the aimpoint appearance model.

5 Conclusion

A novel aimpoint tracking filter was proposed for a wide-band FMCW radar seeker. To resolve the intrinsic data association problem involved with the FMCW seeker, the target range profile was approximately modeled as a function of the length of an aerial target and the closing velocity and used for representing the aimpoint measurement appearance. The resultant model was applied by modifying the association probability of the standard PDA method. This approach made it possible to efficiently separate warhead measurement from others. From the computer simulations, it was confirmed that the proposed approach could provide the superior aimpoint tracking performance compared to the existing methods.

References

[1] S. Josef, "On the feasibility of "hit-to-kill" in the interception of maneuvering targets", *Proc. of American Control Conference*, pp. 3358-3363, 2001.

[2] D. Emeliyanov, E. Rubinovich, and B. Miller, "Information set-based guidance algorithm against a decelerating maneuvering target", *IEEE Trans. Aero. and Electr. Sys.*, vol. 41, no. 1, pp. 65-74, 2005.

[3] J. Shinar and V. Turetsky, "Meeting the challenges of modern interceptor guidance by non-conventional approaches", *Med. Conf. Control and Automation*, pp. 1563-1568, 2009.

[4] D.E. Mosher, "The grand plans", *IEEE Spectrum*, pp. 28-39, 1997.

[5] C.M. Johnson, "Ballistic missile defense radars", *IEEE Spectrum*, pp.32-41, 1970.

[6] J.R. Townsend, *Defense of Naval Task Forces from Anti-ship Missile Attack*, Master Thesis, Naval Postgraduate School, 1999.

[7] K.M. Cuomo, J.E. Pion, and T. Joseph, "Ultrawide-band coherent processing", *IEEE Trans. Antennas and Propagation*, vol. 47, no. 6, pp. 1094-1107, 1999.

[8] G.W. Stimson, *Introduction to Airborne Radar*, Mendham, NJ: Scitech Publishing, 1998.

[9] P.L. Bogler, *Radar Principles with Applications to Tracking Systems*, New York: Wiley, 1990.

[10] H.-H. Ko, K.-W. C, and H.-J. S, "Range resolution improvement for FMCW Radars", *Proc. of European Radar Conference*, pp.352-355, 2008.

[11] T. Kirubarajan and Y. Bar-shalom, "Probabilistic data association techniques for target tracking in clutter", *Proceedings of the IEEE*, vol. 92, no. 3, pp.536-557, 2004.

[12] V. Chen and H. Ling, "Joint time-frequency analysis for radar signal and image processing", *IEEE Signal Processing Magazine*, vol. 16, no. 2, pp.81-93, 1999.

[13] J. Kim, P.K. Menon and E. Ohlmeyer, "Motion models for use with the maneuvering ballistic missile tracking estimators", *AIAA Guid., Nav., and Control Conf.*, pp.1-13, 2010.

[14] W. Farrell, "Interacting multiple model filter for tactical ballistic missile tracking", *IEEE Trans. Aero. and Electr. Sys.*, vol. 44, no. 2, pp.418-426, 2008.

List of Figures

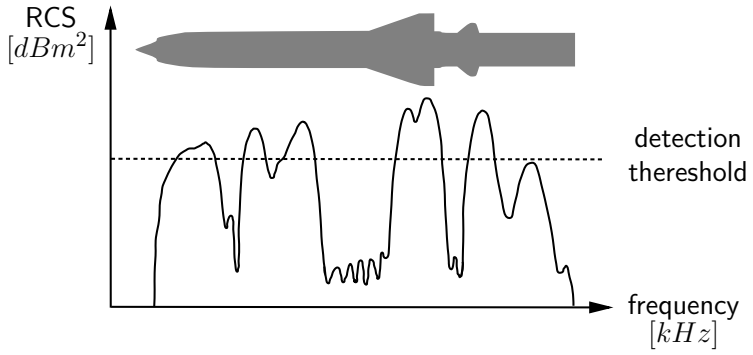

Figure 1: RCS characteristic of an aerial target

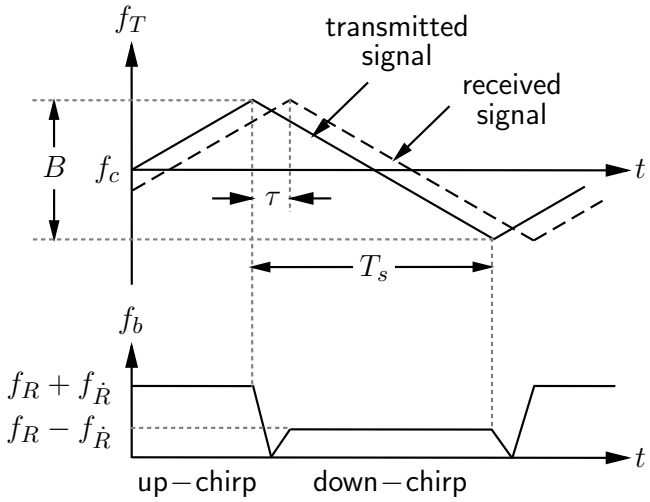

Figure 2: Triangular modulation for an FMCW radar seeker

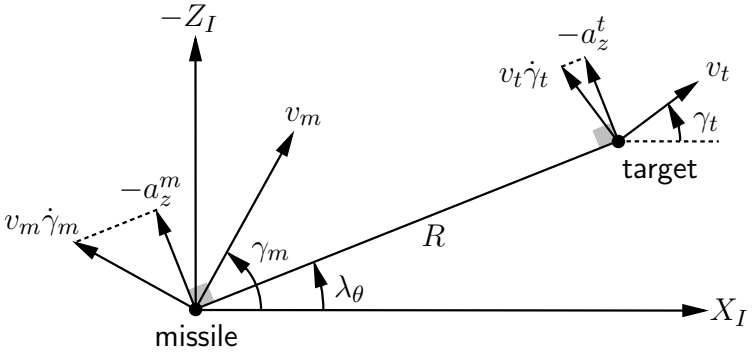

Figure 3: Engagement geometry in vertical plane

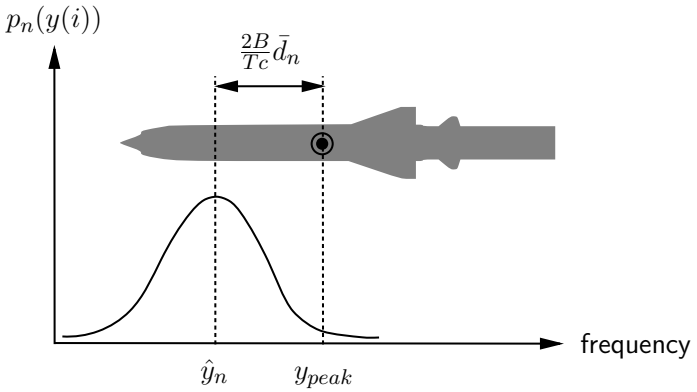

Figure 4: Approximate target range profile

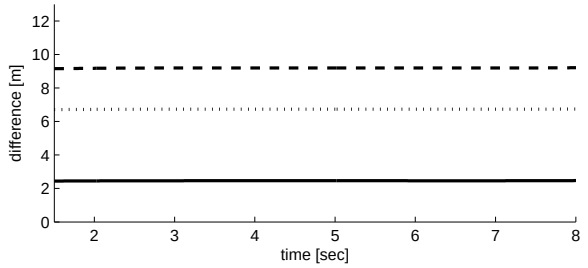

(a) range differences among scatterers

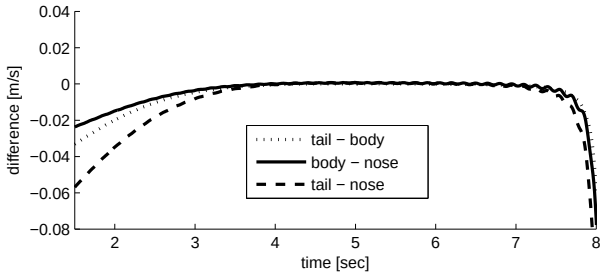

(b) range rate differences among scatterers

Figure 5: Engagement scenario

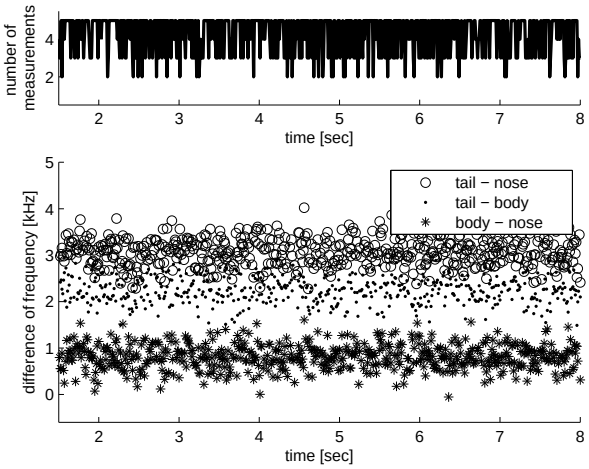

Figure 6: Difference between frequency measurements

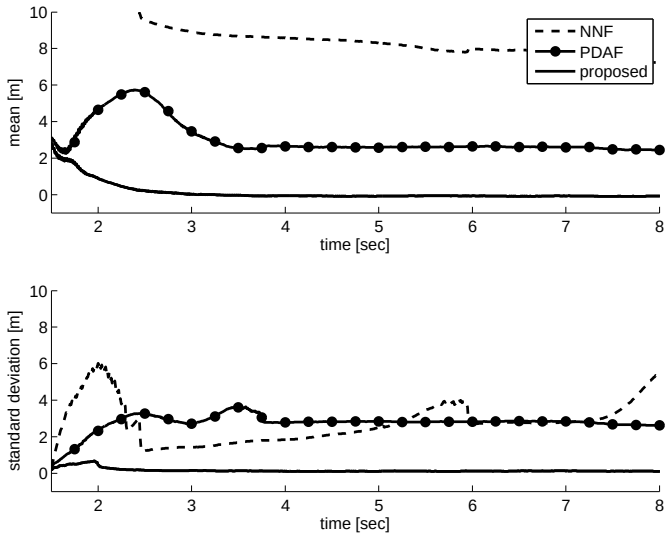

Figure 7: Range estimation error

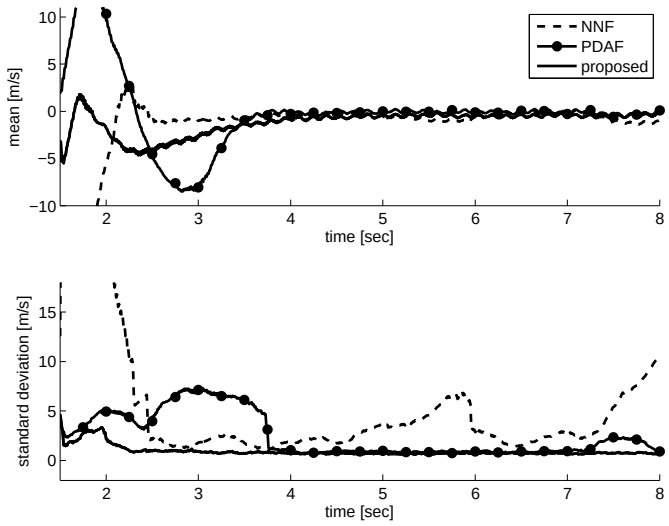

Figure 8: Range rate estimation error

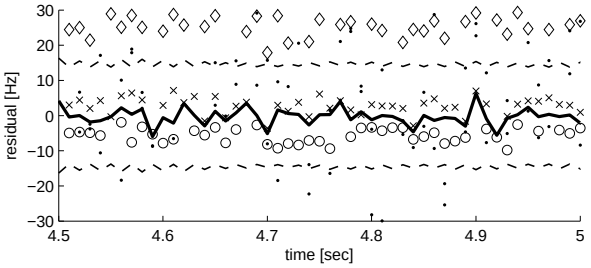

(a) PDAF

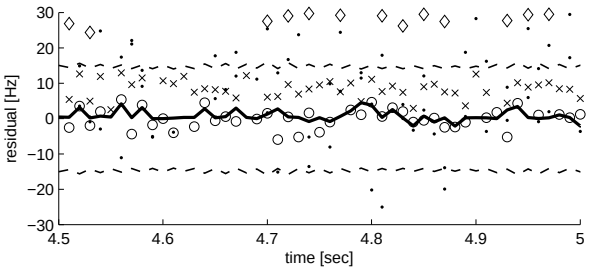

(b) proposed filter

Figure 9: Residues of aimpoint tracking filters: single run (– – : validation gate, — : residue, ∘ : $y_k^n - \hat{y}_{k|k-1}$, × : $y_k^b - \hat{y}_{k|k-1}$, ◊ : $y_k^t - \hat{y}_{k|k-1}$, · : $y_k^c - \hat{y}_{k|k-1}$ where y^n, y^b, y^t, and y^c denote nose, body center, tail, and clutter measurements, respectively)

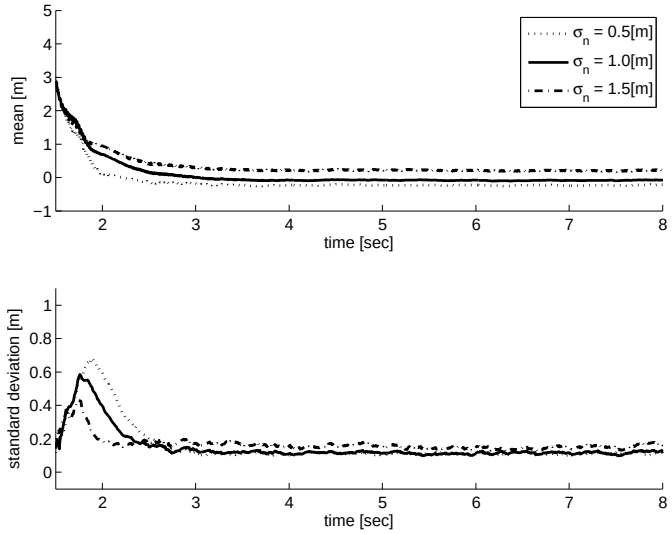

Figure 10: Effects of a uncertain σ_n on the aimpoint tracking